

Supporting Information

Ultra-wideband chromatic aberration-free meta-mirrors

Tong Cai^{a, b, d, §}, Shiwei Tang^{c, §}, Bin Zheng^{a, d, *}, Guangming Wang^b, Wenye Ji^b, Chao Qian^{a, d},

Zuojia Wang^a, Erping Li^{a, d} and Hongsheng Chen^{a, d, *}

^a*Interdisciplinary Center for Quantum Information, State Key Laboratory of Modern Optical Instrumentation, College of Information Science and Electronic Engineering, Zhejiang University, Hangzhou 310027, China*

^b*Air and Missile Defend College, Air force Engineering University, Xi' an, 710051, China*

^c*Department of Physics, Faculty of Science, Ningbo University, Ningbo, 315211, China*

^d*ZJU-Hangzhou Global Science and Technology Innovation Center, Key Lab. of Advanced Micro/Nano Electronic Devices & Smart Systems of Zhejiang, Zhejiang University, Hangzhou 310027, China*

§ These authors contributed equally to this work.

A. Phase modulation principle by using dual-resonant Lorentz model.....	2
B. The working mechanism of the three-layered meta-atom	2
C. Phase modulation principle by using three-resonant Lorentz model.....	4
D. Detailed design of achromatic meta-mirror	5
E. Detailed design of abnormal chromatic meta-mirror.....	7
F. Simulation results of scattered-field patterns for abnormal chromatic meta-mirror.....	8
G. Design of achromatic meta-mirrors at high frequency range	9
H. Design of normal chromatic meta-mirror	16
I. Measurement setup for the designed meta-devices.....	17
J. Comparison of performances between previous literature and our work	18

A. Phase modulation principle by using dual-resonant Lorentz model

In the main text, we discuss how the resonant frequency f_1 affects the reflection phase spectra. Here, we study the effect of f_2 on the reflection phase as shown in Fig. S1(a). The phase spectra vary significantly at high-frequency bands, since the resonance at the high-frequency band is mainly determined by f_2 . And the reflection phase at the low-frequency range is mainly determined by f_1 . By simultaneously changing f_1 and f_2 , we can obtain a reflection phase map including all the reflection response, with the result shown in Fig. S1(b), which can help to design dual-resonant meta-atoms achieving different reflection phase spectra.

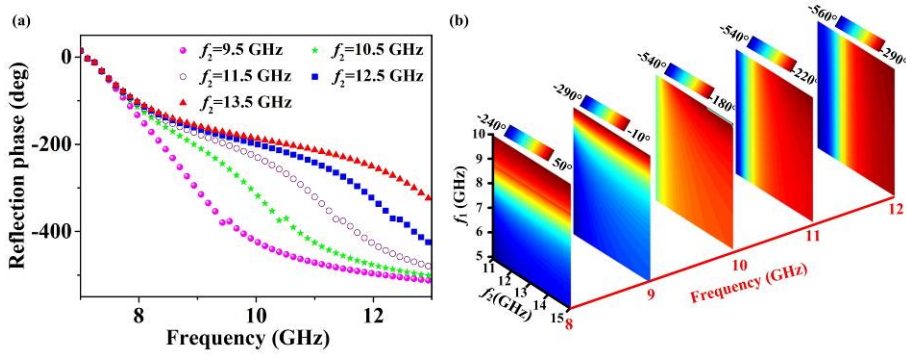


Figure S1 Reflection phase response calculated by dual-resonant Lorentz model. (a) Dependence of reflection phase spectra on f_2 for dual-resonant model computed by TMM with $f_1=7$ GHz, $f_{p1}=6$ GHz and $f_{p2}=7$ GHz. (b) Reflection phase maps as functions of resonant frequency f_1 and f_2 at the frequency band of 8-12 GHz in the step of 1 GHz.

B. The working mechanism of the three-layered meta-atom

Our proposed meta-atom can achieve reflection phase manipulation at a frequency band of 8-12 GHz. In this subsection, we illustrate the underlying physics

via carefully analyzing the EM reflection characteristics of the meta-atom. As already explained in the main text, our proposed meta-atom consists of 4 metallic layers separated by three dielectric layers with its schematic shown in Fig. S2(a). Fig. S2(b) shows the finite-difference-time-domain (FDTD) calculated reflection spectrum of such a meta-atom. The reflection amplitude keeps at a high level of better than 0.95. There are three magnetic resonances for this meta-atom appearing at $f_1=7.54$ GHz, $f_2=10.22$ GHz, and $f_3=12.84$ GHz, respectively. The magnetic resonance f_1 is generated by the interaction between the middle two layers and the lower metallic ground. While the resonance f_2 is due to the interaction between the third metallic bars and the lower metallic layer. The resonance f_3 is mainly generated by the mutual interaction between two metal bars in the upper two layers. We can optimize the structural size to tune the reflection phase spectra via tuning the magnetic resonances with the reflection amplitude remaining nearly unchanged for our meta-atom.

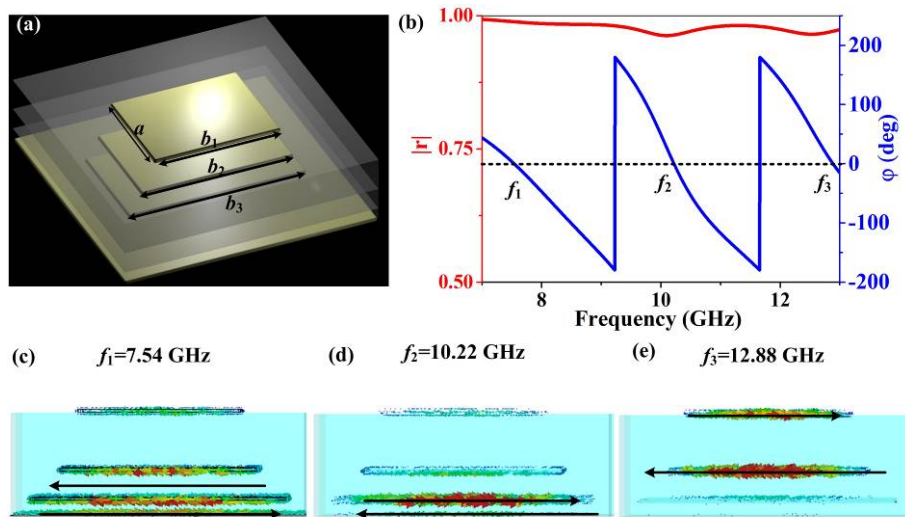


Figure S2. Schematic of three-resonant meta-atom and its EM response. (a) Schematic of meta-atom. (b) FDTD simulated reflection phase and amplitude for meta-atom with $b_1=5.5$ mm, $b_2=6.7$ mm, $b_3=8.7$ mm and $a=6.5$ mm. Current

distributions at the resonant frequencies of (c) f_1 , (d) f_2 and (e) f_3 .

C. Phase modulation principle by using three-resonant Lorentz model

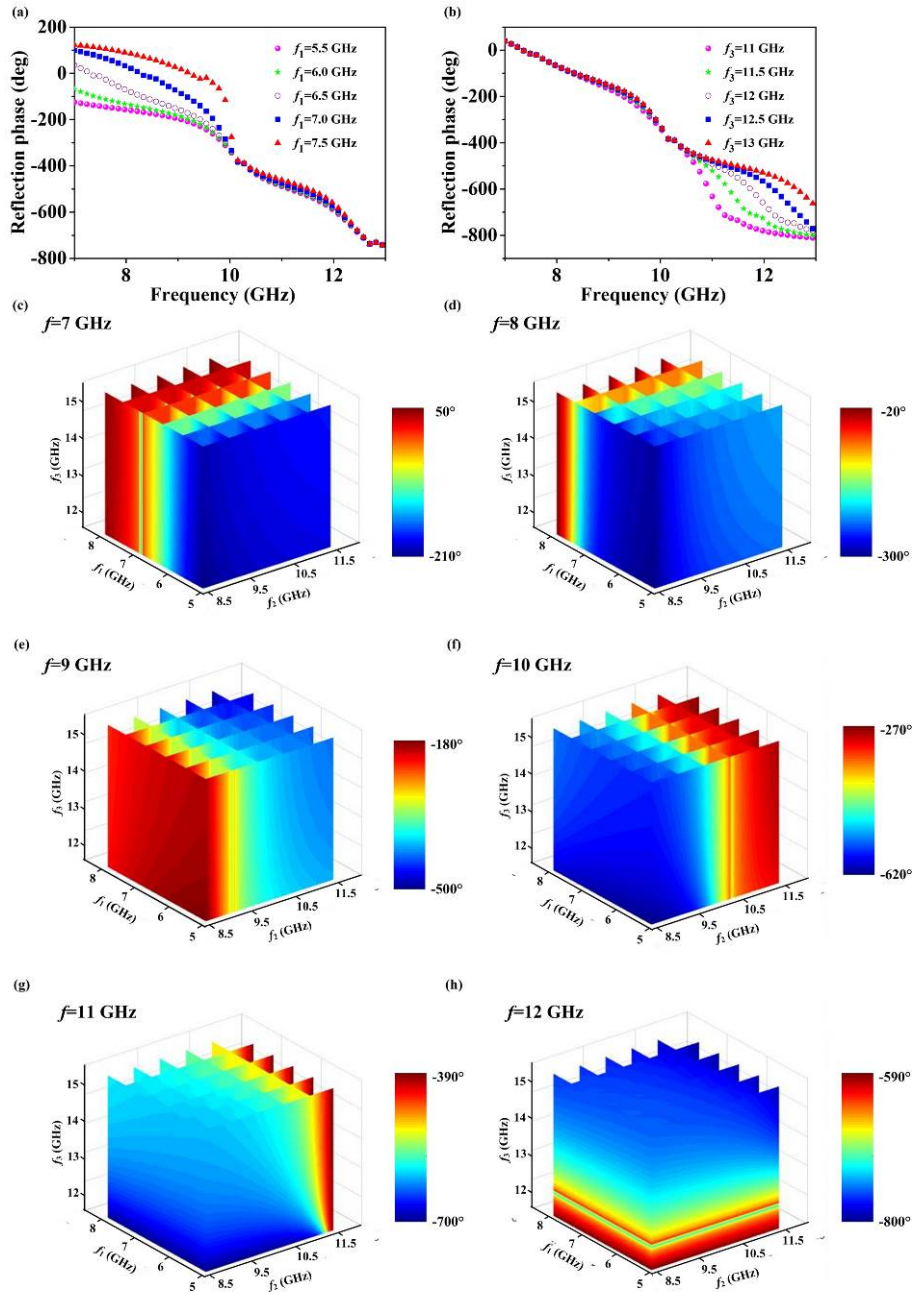


Figure S3 Reflection phase response calculated by the three-resonant Lorentz model.

(a) Dependence of reflection phase spectra on f_1 for a three-resonant model computed by TMM with $f_2=10$ GHz, $f_3=12.9$ GHz, $f_{p1}=5$ GHz and $f_{p2}=4$ GHz and $f_{p3}=6$ GHz. (b)

Dependence of reflection phase spectra on f_3 for three-resonant model computed by TMM with $f_1=7$ GHz, $f_2=10$ GHz, $f_{p1}=5$ GHz and $f_{p2}=4$ GHz and $f_{p3}=6$ GHz. Reflection phase maps as functions of resonant frequency f_1 , f_2 and f_3 at frequency of (c) 7 GHz, (d) 8 GHz, (e) 9 GHz, (f) 10 GHz, (g) 11 GHz and (h) 12 GHz.

The phase variation range is limited by the single and dual resonant model, which can be solved by increasing the number of resonances. We have discussed in the main text that the reflection phase of the three-resonant model can be tuned by changing the resonant frequency f_2 at the middle-frequency band. Figures S3(a) and (b) depict the reflection phase spectra dependences on f_1 and f_3 . We can note that the reflection phase at a low-frequency band can mainly affect by f_1 , while at the high-frequency band by f_3 . To obtain an arbitrary reflection phase spectrum, we should interchange all the three resonances and the reflection phase maps are depicted in Figs. S3(c)-(f). The reflection phases are mainly controlled by f_1 at 7 and 8 GHz, by f_2 at 9, 10 and 11 GHz and by f_3 at 12 GHz. Moreover, we can obtain reflection phase spectra with tailored slopes by tuning these resonances, which is very essential to design frequency-dependent meta-devices. With these maps in hand, we can calculate the resonances quickly and can guide us to design realistic meta-atoms.

D. Detailed design of achromatic meta-mirror

According to Eq. (4) in the main text, an achromatic meta-mirror should exhibit a linear phase spectrum for each meta-atom while the slope of phase profile is different. Multi-resonant Lorentz model provides guidance to design meta-atom with such phase distribution. We firstly calculated the resonant frequencies of each

meta-atom based on the phase maps shown in Fig. S3. Secondly, each meta-atom, composing of a three-layer composite structure, is optimized carefully. The detailed structural sizes are provided in Fig. S4.

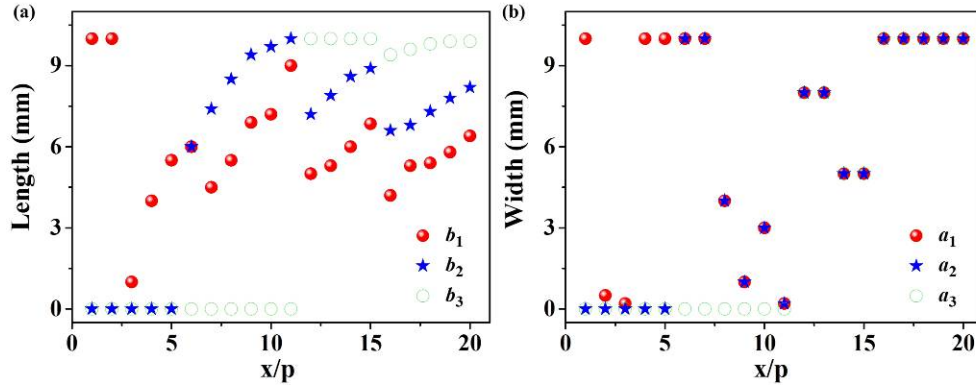


Figure S4 Distributions of structural parameters (a) b_1 , b_2 , b_3 and (b) a_1 , a_2 , a_3 of the achromatic beam deflector studied in Figs. 3 and 4 in the main text. All parameters have the unit of mm.

Figure S5 depicts the reflection amplitudes, reflection phase as well as phase differences between the designed case and the theoretical one. We can note that the reflection amplitude for each meta-atom remains at a high value larger than 0.94 within the operating frequency band, and the loss is caused by the dielectric loss. Meanwhile, the designed phase coincides well with the theoretical case, with the phase differences less than $\pm 10^\circ$ for our meta-device. The high reflection and accurate phase distributions ensure the high efficiency of our meta-device.

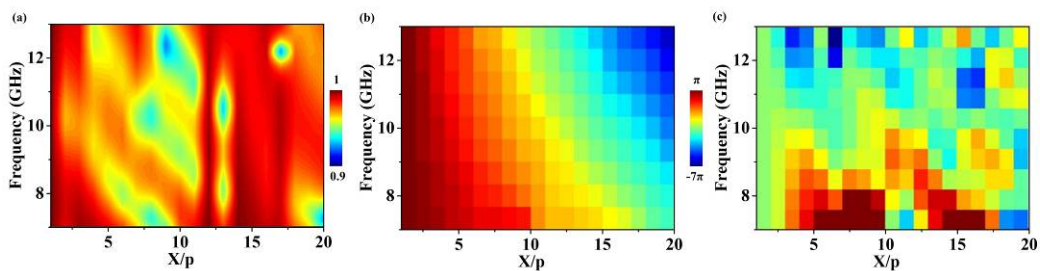


Figure S5 FDTD simulated distributions of (a) reflection amplitude, (b) phase and (c)

phase difference as a function of frequency for the designed meta-mirror studied in Figures 3 and 4 of the main text.

E. Detailed design of abnormal chromatic meta-mirror

Aided by the three-resonant phase maps (Fig. S2), we can obtain the resonant frequencies of each meta-atom to satisfy the required phase distribution shown in Eq. (5) in the main text. Then we tune the parameters of structural size to realize these resonant frequencies. The detailed geometrical parameters (b_1, b_2, b_3 and a_1, a_2, a_3) of all meta-atoms involved in our meta-device are shown in Fig. S6.

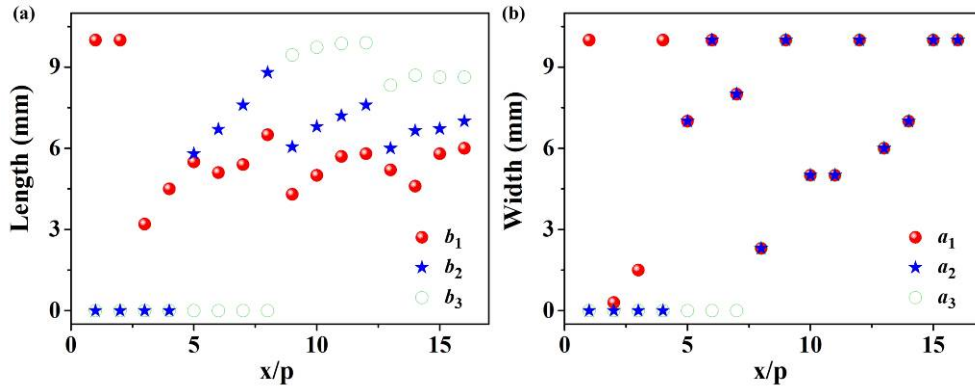


Figure S6 Distributions of structural parameters (a) b_1, b_2, b_3 and (b) a_1, a_2, a_3 of the abnormal chromatic meta-mirror studied in Fig. 5 of the main text. All parameters have the unit of mm.

Figure S7 plots the distribution of reflection amplitude, designed reflection phase as well as phase differences compared with Eq. (5) of the meta-mirror studied in Fig. 5 of the main text. We can see that the reflection phase distribution matches well with the theoretical one. The phase differences at the target frequency band are less than $\pm 15^\circ$, while out of the band, the phase differences increases significantly. The reflection amplitudes of all meta-atoms shown in Fig. S7(c) remain at high values of

$|r_{xx}| > 0.93$ within the frequency band of 8-12 GHz, which guarantees the high efficiencies of our meta-mirror.

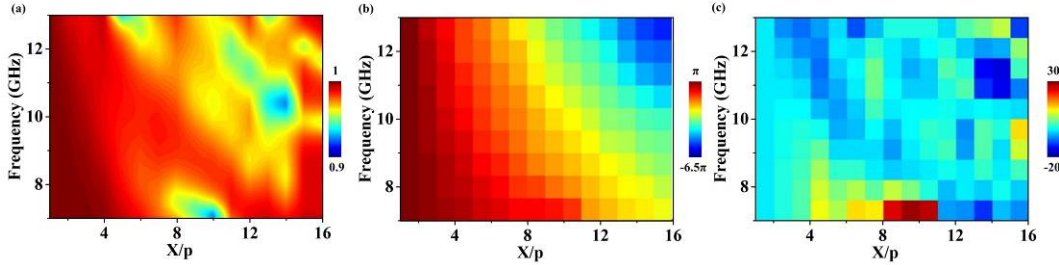


Figure S7 FDTD simulated distributions of (a) reflection amplitude, (b) phase and (c) phase difference as a function of frequency for the designed meta-mirror studied in Fig. 5 of the main text.

F. Simulation results of scattered-field patterns for abnormal chromatic meta-mirror

In Fig. 5(c) of the main text, we plotted the experimentally measured distributions of scattered-field power for our designed abnormal chromatic meta-mirror which is illuminated by normally incident EM waves. Here, we show in Fig. S8 the FDTD simulation results corresponding to these experiments, which are found to have well-reproduced all salient features of the experimental results in Fig. 5(c). Both experimental and FDTD results clearly show that the deflection angle changes as a linear function of frequency, which is quite different from reported beam deflectors. More importantly, almost all the undesired modes are suppressed, indicating the high-efficiency of our meta-device.

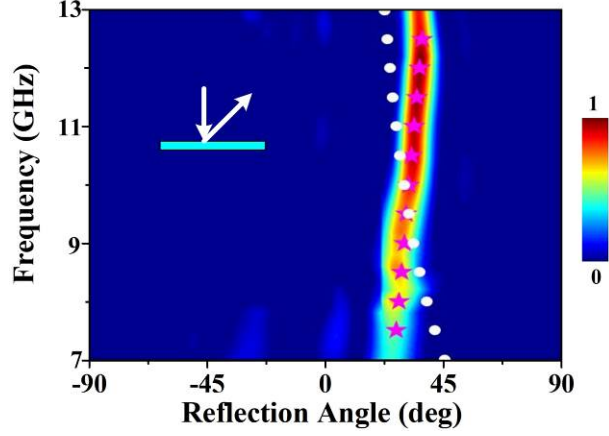


Figure S8 FDTD simulated scattered-field distributions of the abnormal chromatic meta-mirror which is shined by \hat{x} -polarized microwaves. Solid pink stars denote the predefined deflection angles calculated by Eq. (5) in the main text, while the solid white circles denote the deflection angles calculated by generalized Snell's law. All scattered-field values are normalized against the maximum value in the corresponding pattern.

G. Design of achromatic meta-mirrors at high frequency range

We design a microwave *aberration meta-mirror* with *broad bandwidth and high efficiency* in the main text. In fact, our strategy to design chromatic aberration-free metadevices can work not only at the microwave but also at the high frequency band. To show this ability, we designed a THz achromatic meta-mirror and a optical achromatic meta-mirror based on the proposed strategy in the following section.

Firstly, we design a *THz aberration meta-mirror*. The frequency range is chosen from 0.5 THz to 0.8 THz, and the beam deflection angle is set to be 30° . The required phase at the local position of the meta-mirror can be calculated as

$$\varphi_m(r, \lambda_i) = -\frac{2\pi}{\lambda_i} \sin\left(\frac{\pi}{6}\right) N_i p + \varphi_0 = -\frac{\pi}{\lambda_i} N_i p + \varphi_0, \text{ with } N_i \text{ being the } i\text{th number of}$$

meta-atoms and the total number is set as $N=20$. Figure S9(a) depicts the theoretical reflection phase distributions as a function of element number and frequency. The phase is similar with that in microwave meta-mirror in the main text. Then, to satisfy the unique requirement of phases, we retrieved the resonant frequencies and design the corresponding meta-atoms. Similar with the microwave design, the composite meta-atom with four metallic layers and three substrate layers is adopted. Figures S9(b) shows the photographs of the designed achromatic meta-mirror at different layers, and our achromatic sample containing 20×20 meta-atoms and occupying a total area of $2.2 \times 2.2 \text{ mm}^2$. Figure S9(c) retrieves the reflection amplitudes of each meta-atom, which is better than 0.65 within the frequency interval of 0.5-0.8 THz.

Next, we demonstrate the *achromatic* and *high-efficiency* performances of the meta-mirror. The *achromatic* property is considered firstly. The FDTD simulations are performed by shining an \hat{x} -polarized incidence (0.4-0.9 THz) normally onto our meta-mirror, and the angular distributions of scattered waves at the reflection side are calculated with the results shown in Fig. S9(d). It is clear that most of the incident waves are reflected to an identical angle 30° within our target frequency band (0.5-0.8 THz). And other undesired modes are completely suppressed, indicating a high working efficiency of the designed achromatic meta-mirror. While outside the working band, undesired modes increase significantly since the dispersion profile can not satisfy the requirements. Figure S10 depicts the simulated electric field distributions at the frequency interval of 0.5-0.8 THz in the step of 0.1 THz. We can see pure beam bending signature and the exact deflection angles of 30° , which

reinforce the achromatic property of our meta-mirror. The *working efficiency* is quantitatively characterized secondly. Similar with the microwave meta-mirror, the working efficiency is defined as the ratio between the power carried by the desired mode and the incident power at different frequencies. The power taken by the desired mode is calculated by integrating the scattered wave over an appropriate angle region at each frequency. While the incident power is obtained by integrating the scattering modes of a metallic plate with the same size of the meta-mirror. Seeing from Fig. S9(e), the absolute efficiencies of our meta-device are within the range of 75%-84% at the target frequency band of 0.5-0.8 THz. We also estimate the loss of meta-device by using $A(f) = \frac{1}{N} \sum_i 1 - |r_i(f)|^2$, with the results depicted in Fig. S9(f). We can see that the loss is within 5%-13% at our frequency band, which is higher than that in microwave case (~1.5-4%). Despite the increasing plasmonic loss, our meta-mirror exhibits high efficiency and wideband property compared with the reported meta-devices due to the satisfied phase and dispersion distributions within the working frequency range.

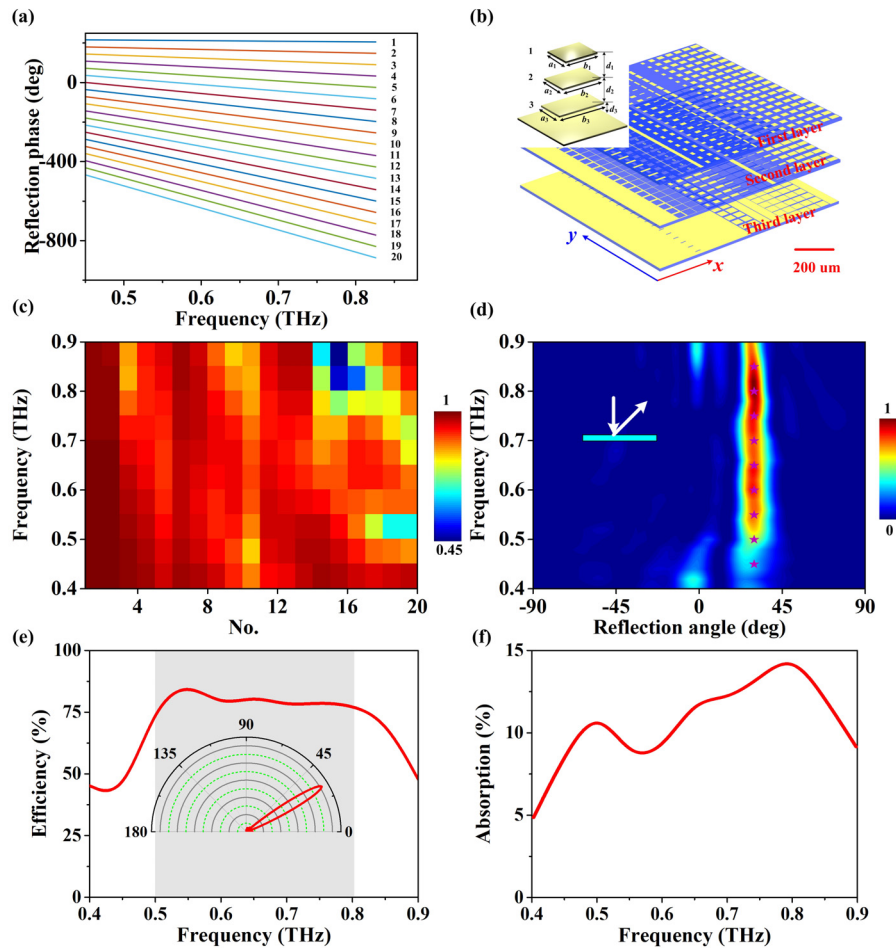


Figure S9 Design and performance of the THz achromatic meta-mirror. (a) Reflection phase distributions of 20 meta-atoms against frequencies. (b) Pictures of the designed sample of meta-mirror. Inset shows the schematics of the meta-atom, which is composed of four metallic layers separated by three polyimide spacers ($\epsilon_r = 3.0 + 0.02i$, $p = 110 \mu\text{m}$, $d_1 = 34 \mu\text{m}$, $d_2 = d_3 = 35 \mu\text{m}$). We treat Gold as lossy metal of conductivity $1.0e6 \text{ S/m}$ in THz regime and with a thickness of 150 nm . (c) Simulated reflection amplitudes of each meta-atom at different frequencies. (d) Simulated scattered-field intensity (color map) versus frequency and detecting angles at reflection space of the metasurface shined by \hat{x} -polarized THz waves. Solid pink stars denote the pre-designed deflection angles. (e) Simulated absolute efficiencies of

the designed achromatic meta-mirror. Inset shows the simulated scattering pattern at 0.65THz. All field values are normalized against the maximum value in the corresponding spectra/patterns. (f) The simulated absorption of the meta-mirror at different frequencies.

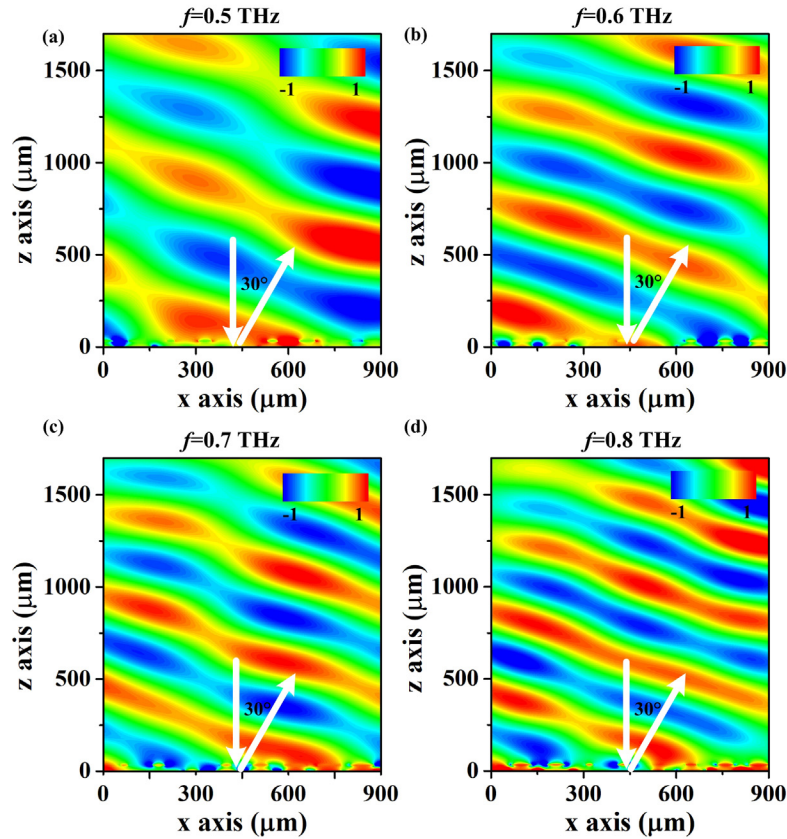


Figure S10 Simulated electric field distributions of our meta-mirror under excitation of \hat{x} -polarized waves at (a) 0.5 THz, (b) 0.6 THz, (c) 0.7 THz and (d) 0.8 THz. All the electric field spectra are normalized against the maximum value at each frequency.

Secondly, we consider to design an optical achromatic meta-mirror. The metal loss increases significantly for the optical meta-devices, especially for those with multi-resonant metallic structures. Therefore, we realize our strategy to tune both *reflection phase* and *dispersion* based on multi-resonant dielectric meta-atoms. Three

kinds of dielectric materials with different thicknesses are optimized to reach the required phase distributions. Due to the dielectric-resonant property, the designed optical meta-mirror can be low-loss, but the price is that its thickness is about $\lambda/2$. Here, the optical wavelength region is chosen from 1150 nm to 1875 nm, and the achromatic deflection angle is set as 20° . The geometry of the designed meta-mirror is shown in Fig. S11(a), and our meta-mirror consists of 18 meta-atoms.

Then we demonstrate the performance of our optical meta-mirror by the full wave simulation. Figure S11(c) depicts the simulated scattering patterns against the reflection angle and the wavelength number. It is observed that nearly all incident power is deflected to the predesigned angles (gray stars in Fig. S11(c)) within the wavelength interval. The absolute efficiency is estimated in the range of 85%-91% between 1150nm to 1875nm by integrating the desired mode and the incident power. The high efficiency is due to the accuracy dispersion within the designed wavelength region and the low-loss property of the multi-resonant dielectric structures. Our results show great superiority than those reported achromatic devices. Figure S11(e) depicts the simulated electric field distributions at the wavelength interval of 1150-1875 nm. Pure beam bending signature are observed clearly within the broad wavelength region, reinforcing the achromatic property and high efficiency of our meta-mirror.

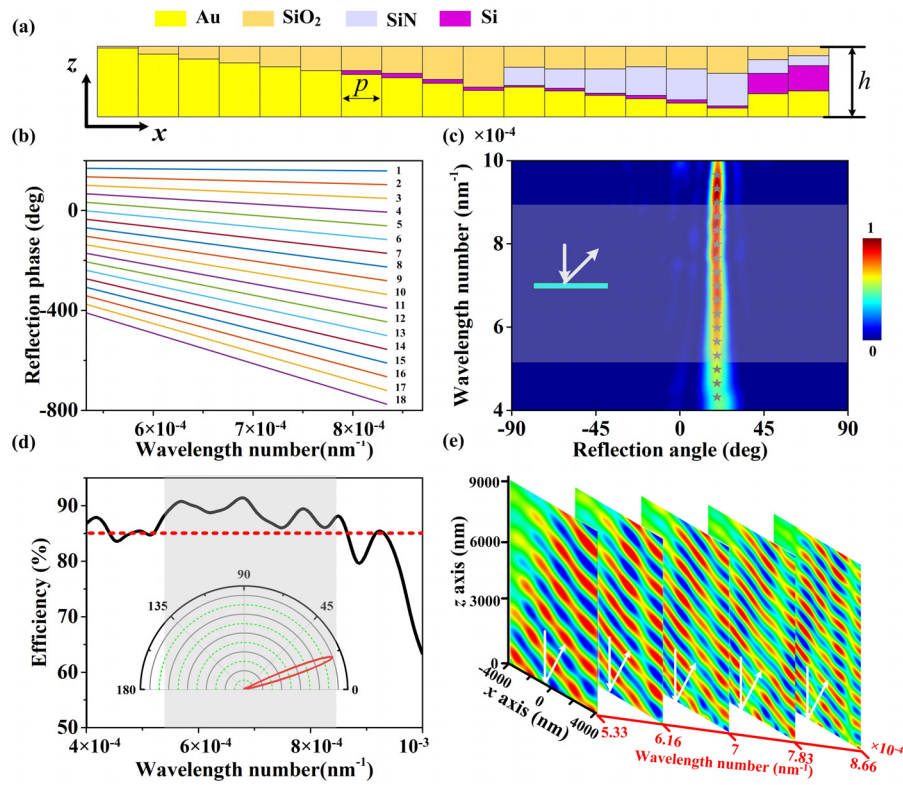


Figure S11 Design and performance of the optical achromatic meta-mirror. (a) Pictures of the designed sample of meta-mirror. Geometry of the designed optical meta-mirror with the period of $p=500$ nm and the thickness of $h=830$ nm. Permittivity of Si (purple), SiO₂ (orange), SiN (light blue) are set as 11.9, 2.1, 4.0, respectively, and a gold layer is adopted at the bottom layer to avoid the transmission of our device. (b) Reflection phase distributions of 18 meta-atoms against wavelength number. (c) Simulated scattered-field intensity (color map) versus wavelength number and detecting angles at reflection space of the metasurface which is shined by \hat{x} -polarized optical waves. Gray stars denote the predesigned deflection angles. (d) Simulated absolute efficiencies of the designed optical meta-mirror. Inset shows the simulated scattering pattern at 1550 nm. All field values are normalized against the maximum value in the corresponding spectra/patterns. (e) Simulated electric field distributions of our meta-mirror under excitation of \hat{x} -polarized waves at different

wavelengths.

H. Design of wideband chromatic meta-mirror

We design an achromatic meta-mirror and an abnormal chromatic meta-mirror by using our three-layered meta-atoms in the main text. These two meta-mirrors exhibit wide bandwidth, high efficiencies and strong dispersion manipulation properties. In fact, our meta-atoms can enhance the bandwidth and efficiency of the conventional narrow band meta-mirror. We set $\varphi_m=60^\circ$ within the band of 8-12 GHz, and thus a supercell consists of 6 meta-atoms with its picture shown in the inset of Fig. S12(a). Figures S12 (a) and 12(b) depict the FDTD simulated reflection spectra of amplitude and phase for the six meta-atoms, respectively. We can see clearly that the amplitudes remain more than 0.95 for our meta-atoms, indicating a high performance of the designed meta-mirror. Moreover, the phase difference keeps at nearly 60° between adjacent meta-atoms, and the deviation is less than $\pm 8^\circ$. With the supercell in hand, we design a normal chromatic meta-mirror by arraying 16 rows with 4 supercells in each row. Shining an \hat{x} -polarized microwave (7-13 GHz) normally onto our meta-mirror, we detected the angular distributions of scattered waves at the reflection side of the metasurface. The simulated results are provided in Fig. S12(c). We can see clearly that most incident power has been deflected to an anomalous angle, which is consistent with the theoretical values (solid pink symbols in Fig. S12(c)). While outside the working band, the specular reflections and other undesirable modes increase significantly. Seeing from the efficiency of the meta-mirror shown in Fig. S12(d), we can obtain that our metasurface exhibits high

efficiencies in a range of 90%-96% within 8-12 GHz, which is much better than the reported meta-mirrors. Inset to Fig. 12(d) shows the simulated radiation pattern at 10 GHz for the meta-mirror.

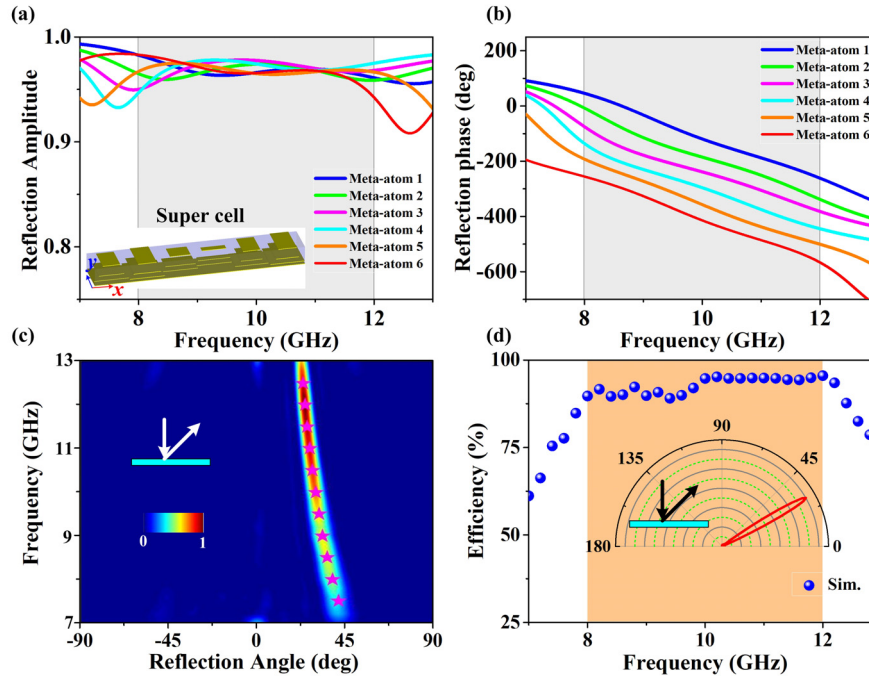


Figure S12 Design and performance of wideband chromatic meta-mirror. FDTD simulated spectra of (a) reflection amplitude and (b) reflection phase for six meta-atoms. Inset to (a) shows the schematic of the supercell. (c) FDTD simulated scattered-field intensity (color map) versus frequency and detecting angles at reflection space of the metasurface shined by \hat{x} -polarized microwaves, and the solid pink stars denote the predefined deflection angles computed by generalized Snell's law. (d) Simulated absolute efficiencies of the normal chromatic meta-mirror, inset to which shows the FDTD simulated radiation pattern at 10 GHz. All field values are normalized against the maximum value in the corresponding spectrum/pattern.

I. Measurement setup for the designed meta-devices

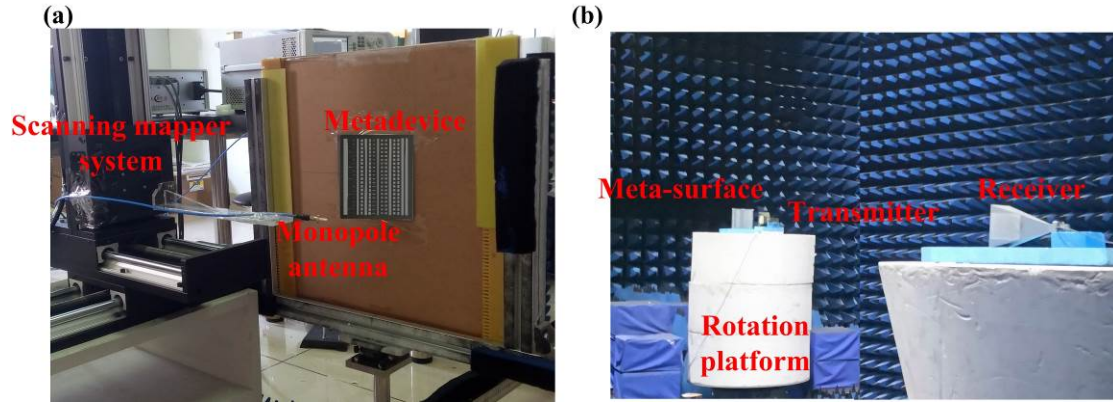


Figure S13 Schematics of the experimental setup for our designed meta-surfaces. (a) Experimental setup to measure $\text{Re}[\vec{E}]$ distributions on xoz plane at the frequency band of 8-12 GHz as the meta-mirrors are illuminated by normally incident \hat{x} -polarized plane waves. (b) Experimental setup to measure far-field scattering patterns of the meta-mirrors.

J. Comparison of performances between previous literature and our work

Here, we make the comparison of performances between the previous research and this work in terms of the bandwidth and operating efficiency, as the results shown in table S1. We can see clear that the proposed chromatic aberration-free meta-mirrors achieve desirable improvements both in very high working efficiency and bandwidth enhancement.

Table S1 Comparison of performances between previous literature and our work

Refs.	Realized functionality	Fractional bandwidth	Operating efficiency	Polarization
[17]	Achromatic lens Achromatic deflector	Three wavelengths (1300nm, 1550nm, 1800nm)	9.8%, 10.3%, 12.6%	LP
[19]	Achromatic lens	Three wavelengths (450nm, 550nm, 650nm)	5.8%-8.7%	LP

[23]	Achromatic lens	Two wavelengths (1180nm, 1680nm)	38%, 52%	LP
[24]	Dispersionless meta-mirror	3.28% (1500-1550nm)	50%-60%	LP
[25]	Achromatic lens Achromatic imaging system	35% (470-670nm)	less than 20%	CP
[26]	Achromatic meta-lens	49% (400-660nm)	~40%	CP
[28]	SPP meta-coupler	5.46% (8.9-9.3 GHz)	50%-73%	LP
[33]	Microwave meta-mirror	7.56% (10.2-11 GHz)	50%-91%	LP
[39]	Spin hall effect	33.3% (10-14 GHz)	50%-90%	CP
[50]	Tunable meta-mirror	46.7% (4.1-6.6 GHz)	~72%	LP
Our work	Achromatic meta-mirror	40% (8-12 GHz)	85%-91%	LP
	Abnormal chromatic meta-mirror			
	THz achromatic meta-mirror	66.7% (0.5-0.8 THz)	75-84%	LP
	Optical achromatic meta-mirror	47.93% (1150-1875nm)	85-91%	LP